Cu_4O_3 thin films deposited by non-reactive rf-magnetron sputtering from a copper oxide target

M. A. Cruz Almazán[a], E. Vigueras Santiago[a], R. López[b,*], S. Hernández López[a], V. Hugo Castrejón Sánchez[b], A. Esparza[c], and C. Encarnación Gómez[d]

[a]*Facultad de Química, Universidad Autónoma del Estado de México, Paseo Colón esquina Paseo Tollocan, Toluca, Estado de México, México.*
[b]*Tecnológico de Estudios Superiores de Jocotitlán, Carretera Toluca-Atlacomulco km 44.8, Ejido de San Juan y San Agustín, Jocotitlán, Edo. México, México.*
[*] *Phone: +527122221259; e-mail: roberto.lopez@tesjo.edu.mx*
[c]*Instituto de Ciencias Aplicadas y Tecnología, Universidad Nacional Autónoma de México, Circuito exterior S/N, Ciudad Universitaria, 04510, México City.*
[d]*Universidad Juárez Autónoma de Tabasco. División Académica Multidisciplinaria de Jalpa de Méndez, Carretera estatal libre Villahermosa-Comalcalco Km 27+000 s/n Rancheria Ribera Alta, 86205, Jalpa de Méndez, Tabasco, México.*

Received 8 November 2020; accepted 31 December 2020

Copper oxide thin films deposited by sputtering are frequently formed by using metal copper targets in reactive atmospheres. In this report, paramelaconite (Cu_4O_3) thin films were deposited by non-reactive rf magnetron sputtering. The target used for sputtering was a copper oxide disk fabricated by oxidation of metal copper at 1000°C for 24 h in the air atmosphere. X-ray diffraction (XRD) results showed that the copper oxide target was mainly composed of cupric oxide (CuO) and cuprous oxide (Cu_2O) crystals. Raman analyses suggested that the surface of the copper oxide disk is composed of a (CuO) layer. XRD measurements performed to the copper oxide thin films deposited by non-reactive rf magnetron sputtering showed that the film is composed of (Cu_4O_3) crystals. However, Raman measurements indicated that the Cu_4O_3 thin films are also composed of amorphous CuO and Cu_2O.

Keywords: Paramelaconite; Cu_4O_3; non reactive sputtering; thermal oxidation.

PACS: 81.15.Cd; 61.82.Fk; 81.65.Mq; 78.30.-j; 68.55.Jk

DOI: https://doi.org/10.31349/RevMexFis.67.495

1. Introduction

There are three main phases of copper oxide: tenorite (CuO), cuprite (Cu_2O), and paramelaconite (Cu_4O_3) [1-3]. The last crystallizes in a tetragonal crystal structure and has a unit cell with three lattice parameters: $a = 5.8370$ Å, $b = 5.8370$ Å, and $c = 9.9320$ Å [4]. Cu_4O_3 is a p-type semiconductor and has a bandgap of 1.75 eV [5]. Although Cu_4O_3 is a metastable phase, it has been recently used in combined with other compounds in some important applications. For example, it has been used in improving catalytic activity of copper oxide-based catalysts [6], as a p-type layer in the fabrication of photodetectors [5], and in antibacterial and cytotoxicity studies [7]. Although Cu_4O_3 can be produced by several techniques such as solvothermal synthesis [8], laser ablation [9], or reactive sputtering [10], it is known that it is difficult to synthesize Cu_4O_3 [11,12]. Copper oxide thin films can be easily deposited by reactive sputtering using metal copper targets [13,14]. A single phase of CuO, Cu_2O, or Cu_4O_3 can be formed by controlling the oxygen flow rate in reactive magnetron sputtering deposition [10]. In the present report, crystalline Cu_4O thin films were obtained by non-reactive rf magnetron sputtering using a home-made copper oxide target, fabricated by thermal oxidation of a metal copper disk.

2. Materials and Methods

Cu_4O_3 thin films were deposited on glass substrates by non-reactive rf magnetron sputtering. The copper oxide targets were fabricated by thermal oxidation of electrolytic copper (C-1100, purity of 99.9 %) disks (two inches of diameter and 500 μm in thickness) (Fig. 1a). Previous to oxidation, the metal copper disks were rinsed in acetone (10 min) and then in ethanol (10 min). Then, they were oxidized at 1000°C for 24 h in the ambient atmosphere using a Thermo-Scientific Thermolyine muffle furnace, model FB1415M. The metal copper disks were placed into the muffle from room temperature to 1000°C, and after oxidation, they were cooled naturally. The thickness of the copper oxide disks was 900 μm (measured with a Mitutyoyo micrometer, model H-2780). The surface of the oxidized disk exhibited the characteristic color of CuO (Fig. 1b). For sputter deposition of copper oxide, the applied voltage and current were 412 V and 8.9 mA, respectively. The copper oxide disc was sputtered in a LEICA MED-020 sputtering system, using Ar plasma at a system pressure of $\sim 6.1 \times 10^{-2}$ mbar. The duration of deposition was 1300 s, and corning glass was used as substrate. The thickness of the sputtered copper oxide thin film (Fig. 1c and 1d) was 370 nm, which was measured using a Sloan Dektak IIA profilometer.

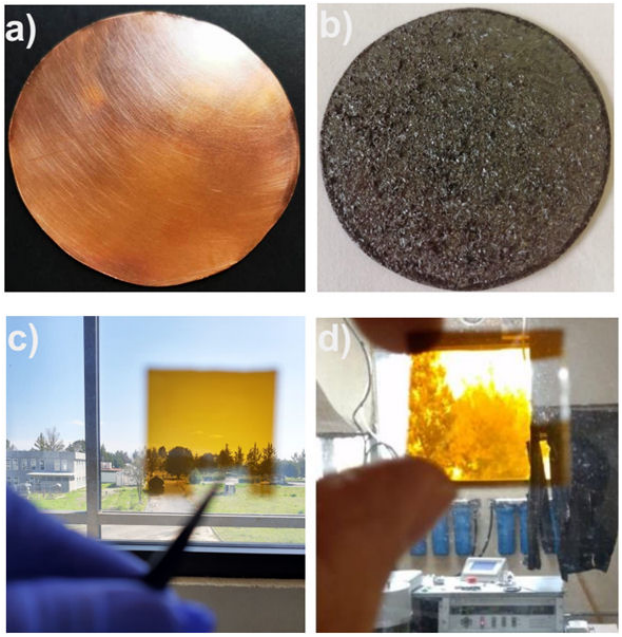

FIGURE 1. a) Photograph of a metal copper disk used for fabrication of the copper oxide target, b) copper oxide target obtained by thermal oxidation of copper, c) and d) top-view of the Cu_4O_3 thin film deposited by non-reactive rf magnetron sputtering.

X-ray diffraction (XRD) measurements were performed with a Bruker D8 Advance diffractometer with radiation of CuKα (1.5406 Å). Raman measurements were recorded using a micro-Raman Horiba Jobin Yvon system (Xplora plus model). A laser ($\lambda = 532$ nm) was used to induce scattering, using a maximum laser power of 10 percent. The laser beam was focused using a 100x lens and also it serves to recollect scattered light. A 600 lines/mm grating was employed; 100 acquisitions were averaged with an exposure time of 5 s each.

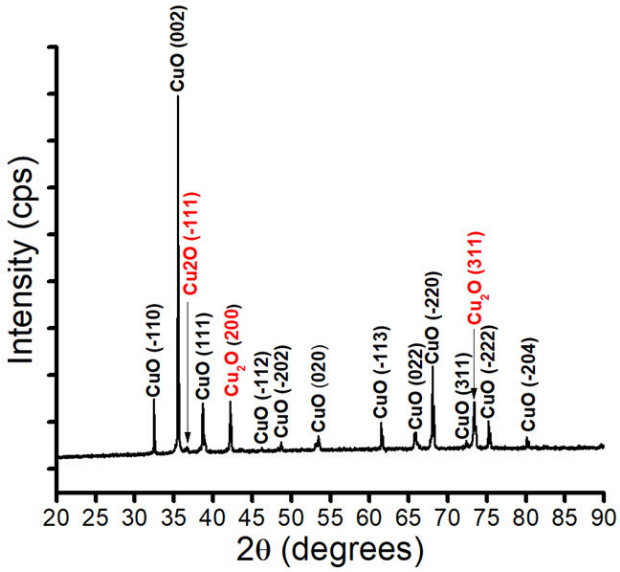

FIGURE 2. XRD diffractogram of a copper oxide target, formed by thermal oxidation at 1000°C for 24 h in air atmosphere.

3. Results and discussion

3.1. Copper oxide target

XRD pattern of copper oxide target fabricated by thermal oxidation of copper at 1000°C for 24 h in the ambient atmosphere is shown in Fig. 2. The 15 peaks observed in the XRD pattern indicate a polycrystalline structure. There are 12 diffraction peaks, at $2\theta = 32.51$, 35.59, 38.76, 46.24, 48.66 , 53.36, 61.53, 65.85, 68.16, 72.40, 75.26, and 80.18°, which match with the (-110), (002), (111), (-112) (-202), (020), (-113), (022), (-220), (311), (-222), and (-204) planes, respectively, of CuO (PDF 00-045-0937). There are also three peaks at $2\theta = 36.65$, 42.18, and 73.43° which correspond to the (111), (200), and (311) planes, respectively, of Cu_2O (PDF 00-005-0667). No peak are corresponding to metal copper. The structure of the disk is thus composed of a mixture of CuO and Cu_2O crystals, which is commonly observed in growth, synthesis, or even in thin film deposition of copper oxide by different methods such as thermal oxidation or sputtering [14,15]. Table I shows the full width at half maximum (FWHM) values calculated for all diffraction peaks observed in the XRD pattern of Fig. 2. The value of the FWHMs for peaks of the CuO phase are in the range of 0.06551-0.21978°, and those of the Cu_2O phase in that of 0.19098-0.25649°. FWHMs for nanostructured CuO or CuO thin films have been previously found in higher values than those reported here, which indicates that the bulk of the copper oxide disk exhibits a crystalline structure [16,17].

Raman measurements were performed at three different zones of the copper oxide disk (Fig. 3a). The zone labeled as z1 indicates any point through the surface of the copper oxide disk. Raman spectrum of z1 is shown in Fig. 3b. There are three sharp bands centered at 294, 342, and 628 cm^{-1}, which agree with the three Raman active modes (A_g + 2B_g) of CuO [18]. Also, there a weak broadband of about 100 cm^{-1}, which has been previously associated non-stoichiometry and defects in Cu_2O [19,20]. Thus, the surface

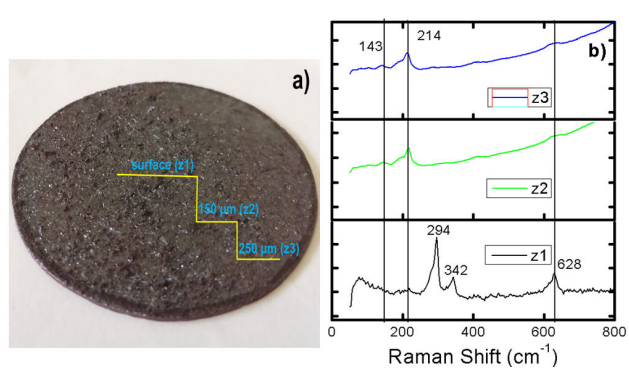

FIGURE 3. a) Photograph of the copper oxide disk where the depth profile used for Raman measurements is observed. b) Raman spectra of measurements performed at the surface and in the bulk of the copper oxide disk.

TABLE I. FWHMs calculated for the fifteen peaks of the XRD pattern of the copper oxide target, formed by thermal oxidation at 1000°C for 24 h in the air atmosphere.

	Plane											
CuO	(-110)	(002)	(111)	(-112)	(-202)	(020)	(-113)	(022)	(-220)	(311)	(-222)	(-204)
FWHM	0.13307	0.14777	0.21978	0.20723	0.16603	0.19891	0.08673	0.16729	0.09425	0.06551	0.12098	0.09934
Cu_2O	(111)	(200)	(311)									
FWHM	0.25649	0.19098	0.19586									

of the copper oxide disk is mainly composed of CuO. The z2 label indicates a measurement zone into the disk at a depth of about 150 μm. There are two Raman bands centered at 143 and 214 cm^{-1}, which correspond to Cu_2O modes [21]. There is also a broad and weak CuO band at around 628 cm^{-1}. The Raman spectrum obtained by measuring at a depth of about 250 μm (z3 zone) exhibits the same three bands observed in the z2 zone. Thus, according to XRD and Raman measurements, the bulk of the copper oxide target is mainly composed of Cu_2O and a surface crystalline layer of CuO.

3.2. Cu_4O_3 thin films

Copper oxide thin films were deposited by non-reactive rf-magnetron sputtering. According to XRD and Raman measurements performed to the copper oxide target, the deposition was achieved by sputtering to the CuO layer on the surface of the copper oxide disk. XRD pattern of sputtered copper oxide thin film is shown in Fig. 4. There are only two peaks at $2\theta = 43.66$ and 63.97°, which correspond to (220) and (400) planes, respectively, of the Cu_4O_3 phase of copper oxide (PDF 00-033-0480). The FWHM of the (220) peak (0.33696°) is smaller than that of (400) peak (0.73691°), which indicates that the average crystal size (estimated by the Scherrer equation) is higher for the (220) peak than that of the

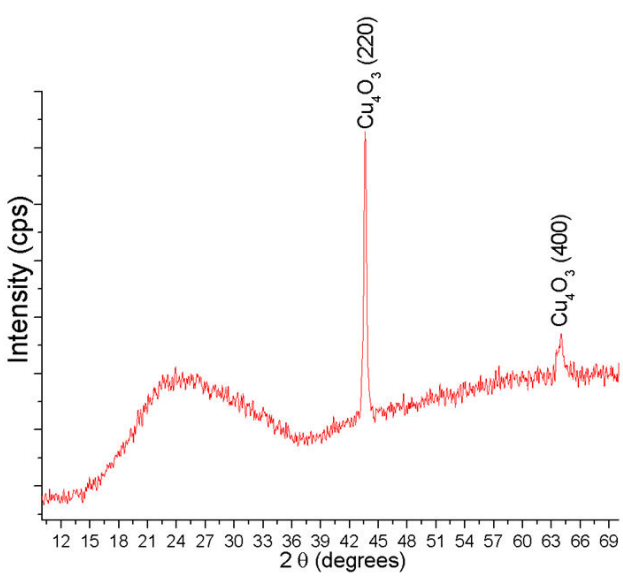

FIGURE 4. XRD pattern of the Cu_4O_3 thin film deposited by non-reactive rf magnetron sputtering of copper oxide.

(400) peak (26.52 and 13.27 nm, respectively) [22]. Also, since the intensity of the (220) peak is about six times higher than that of the (400) one, the Cu_4O_3 thin film exhibits a preferred orientation along the (220) plane. The broadband from $2\theta = 14°$ to $2\theta = 37°$ is the characteristic amorphous band of the glass substrate. This band appeared due to the low thickness of the Cu_4O_3 film. The structural characteristics of the copper oxide target and Cu_4O_3 thin films are shown in Table II. For crystal size calculation using the Scherrer equation ($D = k\lambda/\beta\cos\theta$), D is the crystallite size; K is the shape constant, λ is the CuK radiation, β is the full width at half maximum, and θ is the diffraction angle. Dislocation density (δ) was obtained as shown in Eq. (1) [23]:

$$\delta = \frac{n}{D^2} \tag{1}$$

where n is a factor, which gives the minimum dislocation density when is equal to unity. The distortion degree by variation of the d-spacing within or between crystal domain was calculated by microstrain (ε), as shown in Eq. (2) [24]:

$$\varepsilon = \frac{\beta}{4\tan\theta}. \tag{2}$$

It can be observed that Cu_4O_3 thin films exhibit a smaller crystal size than the copper oxide target, and, consequently, an increment in the microstrain and dislocation density is produced during the formation of the Cu_4O_3 thin films.

Raman spectra of the Cu_4O_3 thin film was performed in three different zones: at the top (point2), at the center (center), and at the bottom of the surface of the thin film (point1) (inset of Fig. 5). There are five main Raman modes in each spectrum of Fig. 5, although peak positions, intensities, and the width of the bands are not identical in all spectra. These variations suggest that the composition of the Cu_4O_3 thin film is inhomogeneous across all its surface. The peak of about 213 cm^{-1} corresponds to Cu_2O mode [25]. The peaks of about 272 and 603 cm^{-1} correspond to CuO modes [26]. The peaks about 323 and 545 cm^{-1} correspond to Cu_4O_3 modes [27].

TABLE II. Crystallite size, dislocation density, and micro-strain of the copper oxide and the Cu_4O_3 thin films.

Sample	D (nm)	$\delta \times 10^{-4}$ (nm^{-2})	$\varepsilon \times 10^{-4}$
Copper oxide target	54.89	3.318	20.698
Cu_4O_3 thin film	26.52	16.126	37.468

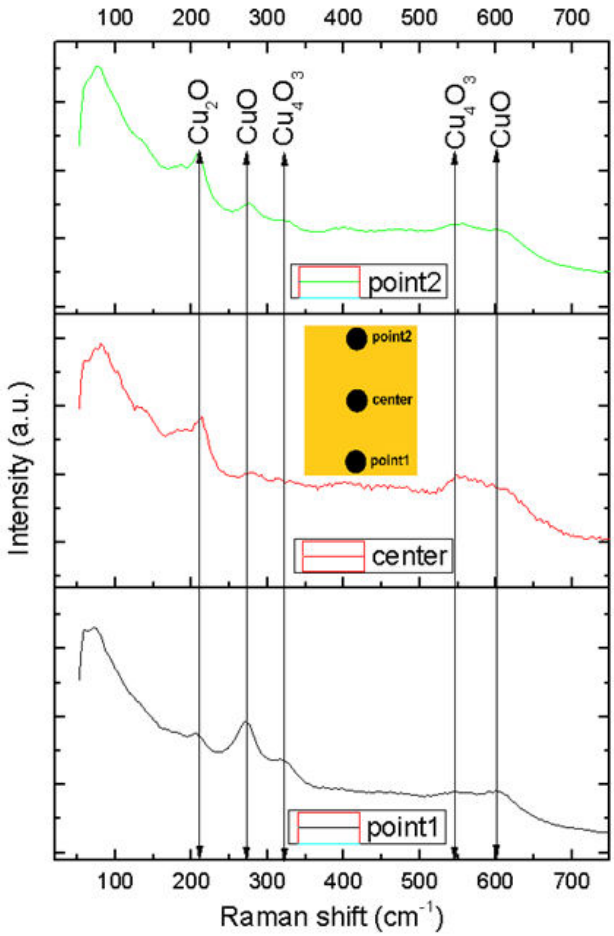

FIGURE 5. Raman spectra of the Cu_4O_3 thin film deposited by non-reactive rf magnetron sputtering of copper oxide. Measurements were performed at three points of the surface of the film (inset): at the the top (point2), at center (center), and the bottom (point1).

XRD results showed a pattern exhibiting only Cu_4O_3 peaks, and Raman measurements suggest that a mixture of CuO, Cu_2O, and Cu_4O_3 phases are present in the structure of the thin film. The bands of the three phases of copper oxide (CuO, Cu_2O, and Cu_4O_3) observed in Raman spectra of the thin film deposited by non-reactive rf-magnetron sputtering are very broad, particularly those that were obtained from the "center" and the "point2" zones. This may be associated with a poor crystalline quality of the thin films.

4. Conclusions

Cu_4O_3 thin films were deposited by non-reactive rf-magnetron sputtering using a copper oxide target, which was obtained by thermal oxidation of copper. From XRD and Raman analyses, deposition of the Cu_4O_3 thin films was achieved by sputtering to the surface CuO layer of the target. XRD measurements indicated that only Cu_4O_3 crystals are present in the structure of the thin films. However, the broad bands of CuO and Cu_2O observed in Raman spectra revealed a bulk composed of a mixture of the three copper oxide phases.

1. R. Dey Dolai, S. Das, S. Hussain, R. Bhar, and A.K. Pal, Cupric oxide (CuO) thin films prepared by reactive d.c. magnetron sputtering technique for photovoltaic application, *Journal of Alloys and Compounds*, **724** (2017) 456. `https://doi.org/10.1016/j.jallcom.2017.07.061`

2. A.O Musa, T Akomolafe, and M.J Carter, Production of cuprous oxide, a solar cell material, by thermal oxidation and a study of its physical and electrical properties, *Solar Energy Materials and Solar Cells*, **51** (1998) 305. `https://doi.org/10.1016/S0927-0248(97)00233-X.`

3. Zhelong Jiang, Shiliang Tian, Shuqi Lai, Rebecca D. McAuliffe, Steven P. Rogers, Moonsub Shim, and Daniel P. Shoemaker, Capturing Phase Evolution during Solvothermal Synthesis of Metastable Cu_4O_3, Chemistry of Materials 28 (2016) 3080. DOI: `10.1021/acs.chemmater.6b00421`

4. D. Smith, *et al*., Penn State University, University Park, Pennsylvania, USA., ICDD Grant-in-Aid, (1979).

5. Kim, H.-S., Kumar, M. D., Park, W.-H., Patel, M., and Kim, J. Cu_4O_3 -based all metal oxides for transparent photodetectors. *Sensors and Actuators A: Physical*, **253** (2017) 35. doi:`10.1016/j.sna.2016.11.020`

6. N. Martić, *et al.*, Paramelaconite-Enriched Copper-Based Material as an Efficient and Robust Catalyst for Electrochemical Carbon Dioxide Reduction. *Advanced Energy Materials*, **9** (2019) 1901228. doi:`10.1002/aenm.201901228`

7. J. Thanuja, Udayabhanu, Nagaraju, G., Raja Naika H, Biosynthesis of Cu_4O_3 nanoparticles using Razma seeds: application to antibacterial and cytotoxicity activities. *SN Appl. Sci.* **1** (2019) 1646. `https://doi.org/10.1007/s42452-019-1556-3`

8. Zhelong Jiang, Shiliang Tian, Shuqi Lai, Rebecca D. McAuliffe, Steven P. Rogers, Moonsub Shim, and Daniel P. Shoemaker, Capturing Phase Evolution during Solvothermal Synthesis of Metastable Cu_4O_3, *Chemistry of Materials*, **28** (2016) 3080. DOI: `10.1021/acs.chemmater.6b00421`

9. M. Arreguín-Campos *et al.*, Synthesis of paramelaconite nanoparticles by laser ablation. *Journal of Laser Applications*, **30** (2018) 012012. doi:10.2351/1.4986981
10. J.F. Pierson, A. Thobor-Keck, A. Billard, Cuprite, paramelaconite and tenorite films deposited by reactive magnetron sputtering, *Applied Surface Science*, **210** (2003) 359. https://doi.org/10.1016/S0169-4332(03)00108-9.
11. D.S. Murali, S. Aryasomayajula, Thermal conversion of Cu4O3 into CuO and Cu2O and the electrical properties of magnetron sputtered Cu4O3 thin films. *Appl. Phys. A* **124** (2018) 279. https://doi.org/10.1007/s00339-018-1666-6
12. Li, F., Chang, Q., Li, N., Xue, C., Liu, H., Yang, J., Shengliang H., Wang, H., Carbon dots-stabilized Cu4O3 for a multi-responsive nanozyme with exceptionally high activity. *Chemical Engineering Journal*, **394** (2020) 125045. doi:10.1016/j.cej.2020.125045
13. L. Radjehi, *et al.*, Effect of vacuum annealing on the structural and optical properties of sputtered Cu_4O_3, thin films, *Surface Engineering*, **35** (2020) 1. doi:10.1080/02670844.2020.1753397
14. Yahya Alajlani, Frank Placido, Anders Barlow, Hin On Chu, Shigeng Song, Saeed Ur Rahman, Robert De Bold, Des Gibson, Characterisation of Cu_2O, Cu_4O_3, and CuO mixed phase thin films produced by microwave-activated reactive sputtering, *Vacuum*, **144** (2017) 217. https://doi.org/10.1016/j.vacuum.2017.08.005.
15. Qing Yang, Zhiang Guo, Xiaohong Zhou, Juntao Zou, Shuhua Liang, Ultrathin CuO nanowires grown by thermal oxidation of copper powders in air, *Materials Letters*, **153** (2015) 128. https://doi.org/10.1016/j.matlet.2015.04.045.
16. V. S. Levitskii, *et al.*, Raman spectroscopy of copper oxide films deposited by reactive magnetron sputtering. *Technical Physics Letters*, **41** (2015) 1094. DOI: 10.1134/S106378501511022X
17. Y. Wang *et al.*, Tuning the structure and preferred orientation in reactively sputtered copper oxide thin films. *Applied Surface Science*, **335** (2015) 85. https://doi.org/10.1016/j.apsusc.2015.02.028
18. M.A. Dar, Q. Ahsanulhaq, Y.S. Kim, J.M. Sohn, W.B. Kim, H.S. Shin, Versatile synthesis of rectangular shaped nanobat-like CuO nanostructures by hydrothermal method; structural properties and growth mechanism, *Applied Surface Science*, **255** (2009) 6279.
19. V.S. Levitskii, *et al.*, spectroscopy of copper oxide films deposited by reactive magnetron sputtering. *Technical Physics Letters*, **41** (2015) 1094. DOI: 10.1134/S106378501511022X
20. Y. Wang *et al.*, Tuning the structure and preferred orientation in reactively sputtered copper oxide thin films. *Applied Surface Science*, **335** (2015) 85. https://doi.org/10.1016/j.apsusc.2015.02.028
21. S. R. Adilov, *et al.*, Studying the composition and structure of films obtained by thermal oxidation of copper. *Glass Phys Chem* **43** (2017) 272. https://doi.org/10.1134/S1087659617030026
22. D. Santos-Cruz, S.A. Mayén-Hernández, F. de Moure-Flores, J. Campos-Álvarez, Mou Pal, J. Santos-Cruz, CuOX thin films by direct oxidation of Cu films deposited by physical vapor deposition, *Results in Physics*, **7** (2017) 4140. https://doi.org/10.1016/j.rinp.2017.10.022.
23. H.P. Klug , L.E. Alexander *X-ray diffraction procedures for polycrystalline and amorphous materials*. (John Wiley & Sons, New York 1974).
24. A. Baig, *et al*. Relationships Among Carbonated Apatite Solubility, Crystallite Size, and Microstrain Parameters. *Calcif Tissue Int* **64** (1999) 437. https://doi.org/10.1007/PL00005826
25. M. A. M. Patwary, *et al.*, Effect of oxygen flow rate on properties of Cu_4O_3 thin films fabricated by radio frequency magnetron sputtering. *Journal of Applied Physics*, **127** (2020) 085302. doi:10.1063/1.5144205
26. Deng, Y., Handoko, A. D., Du, Y., Xi, S., and Yeo, B. S., In Situ Raman Spectroscopy of Copper and Copper Oxide Surfaces during Electrochemical Oxygen Evolution Reaction: Identification of CuIII Oxides as Catalytically Active Species. *ACS Catalysis*, **6** (2016) 2473. doi:10.1021/acscatal.6b00205
27. L. Debbichi, M. C. Marco de Lucas, J. F. Pierson, and P. Krüger, Vibrational Properties of CuO and Cu_4O_3 from First-Principles Calculations, and Raman and Infrared Spectroscopy, *The Journal of Physical Chemistry C* **116** (2012) 10232. DOI: 10.1021/jp303096m